Assessing Antisite Defect and Impurity Concentrations in Bi_2Te_3 Based Thin Films by High-Accuracy Chemical Analysis

Nicola Peranio, Markus Winkler, Michael Dürrschnabel, Jan König, and Oliver Eibl*

In Bi_2Te_3-based materials charge-carrier densities are determined by antisite defects and controlling these defects is a key issue for thermoelectric and topological insulator materials. Bi-Te thin films with high-quality thermoelectric properties are deposited using a nano-alloying approach by molecular beam epitaxy (MBE) and sputtering. The in-plane transport properties are measured at room temperature as a function of charge-carrier density. High-accuracy chemical analysis by wavelength-dispersive X-ray spectrometry (WDX) is applied for the first time to these Bi_2Te_3-based thin films. The acquisition conditions for WDX spectrometry are established using Monte Carlo simulations for the electron trajectories, which guarantees a high lateral resolution and rules out stray radiation generated in the substrate of the films. In contrast to energy-dispersive X-ray spectrometry (EDX), which is usually applied, WDX offers unprecedented accuracy for measuring antisite defect concentrations and thus has a high impact on improving the quality of thin films. The charge-carrier densities are calculated from the WDX results according to the point-defect model of Miller and Li and the thermopower and electrical conductivity are calculated for different charge-carrier densities by solving the linearized Boltzmann transport equation. A good quantitative agreement is found for the dependence of the thermopower on stoichiometry, whereas the electrical conductivity is sensitively affected by contaminants.

1. Introduction

Bi_2Te_3-based compounds yield the highest thermoelectric figure of merit *ZT* of around 1 at room temperature.[1] These compounds have a large number of structural and chemical degrees of freedom that affect the thermoelectric properties. This requires a systematic approach in terms of materials synthesis, structural characterization, thermoelectric characterization, and theory.

Hicks and Dresselhaus[2] predicted an increase of the thermoelectric figure of merit beyond 1 for nanomaterials and Cornett and Rabin[3] recently extended that model by involving the contributions of multiple subbands. The report of Venkatasubramanian et al. about Bi_2Te_3/Sb_2Te_3 superlattices with spectacular *ZT* values of 2.4[4] was a boost for the fabrication of Bi_2Te_3-based thin films and superlattices. However, these outstanding *ZT* values were not reached again for thin films and superlattices, not by other groups[5–8] nor by us and our collaborators.[9–14]

We realized[10] that in thin films antisite defects and other point defects are *ZT* limiting factors of key importance and the role of point defects was not considered in the pioneering work of Hicks and Dresselhaus.[2] The point-defect density is controlled by the temperature; and thin films, in particular, are exposed to maximum temperatures in the range between 250 °C to 350 °C,[10] whereas for bulk materials the temperature at the congruent melting point of 585 °C[1] is relevant. The hole conduction in single-crystalline Bi_2Te_3 bulk materials grown close to equilibrium conditions with a tellurium mole fraction of less or equal to 60 at%[1,15] was explained by acceptor-like Bi_{Te} antisite defects by Miller and Li,[16] who determined the antisite defect density by high-accuracy density measurements.

In Bi_2Te_3 the charge-carrier density is determined by the antisite defects and the antisite defect concentration is determined by stoichiometry. Therefore, precise chemical analysis of the films is of crucial importance for understanding their thermoelectric properties. In our previous reports[9–14] we used energy-dispersive X-ray spectrometry (EDX) for chemical analysis. However, the antisite defect concentration is smaller than the accuracy of quantitative EDX measurements. Even for Sb_2Te_3 with defect concentrations as high as about 10^{20} cm^{-3}[1,17] the point-defect density cannot be measured by EDX.

In this work wavelength-dispersive X-ray spectrometry (WDX) is used for high-accuracy chemical analysis, as its energy resolution and detection limit is about 10 times better than that of EDX spectrometry.[18] This technique has successfully been used by our group for detecting variations in stoichiometry in Bi_2Te_3 bulk materials.[19,20] In this work, WDX will be applied to thin films to determine: i) mean chemical compositions, ii) variations in stoichiometry,

Dr. N. Peranio, M. Dürrschnabel, Prof. Dr. O. Eibl
Eberhard Karls Universität Tübingen
Institut für Angewandte Physik
Auf der Morgenstelle 10, Tübingen 72076, Germany
E-mail: nicola.peranio@uni-tuebingen.de
M. Winkler, Dr. J. König
Fraunhofer Institut Physikalische Messtechnik
Heidenhofstrasse 8, Freiburg 79110, Germany

DOI: 10.1002/adfm.201300606

iii) oxygen contamination, and iv) Ar implantation in sputtered films. The effect of non-stoichiometry and contamination on the defect concentrations and transport properties will be discussed based on these high-accuracy chemical analyses. The discussion will also include calculated electronic transport coefficients obtained by solving the linearized Boltzmann transport equation using the BoltzTraP code of Madsen and Singh.[21,22]

2. Results

2.1. In-Plane Thermoelectric Properties

In this paper the thermoelectric properties of the thin films will be correlated with the chemical composition of the films that were measured by high-accuracy WDX spectrometry in an electron probe microanalyzer (EPMA). The measurements will be explained in more detail in the following section. The thermoelectric data of the films selected for this paper were already explained in some detail in the literature as quoted in **Table 1**. We will therefore only highlight the most important results relevant for this study.

Table 2 summarizes transport properties of films grown by a nano-alloying approach using a molecular beam epitaxy (MBE) setup or sputtering. For molecular beam epitaxy a stoichiometric series was prepared, whereas for the sputtered films only specific compositions were synthesized close to the stoichiometric point. The charge-carrier density of nominally stoichiometric films (#1, #2, #3, #6, #7) could be controlled and set in the range of 3×10^{19} cm^{-3}, in other words, lower than usually obtained in bulk samples.[1] Note that different from the bulk samples, MBE-prepared Bi_2Te_3 films were n-type only although Bi-rich films were prepared. Hole-conducting films were realized by depositing Sb_2Te_3. The control of the charge-carrier density is of utmost importance for synthesizing high-quality thermoelectric materials and determining and controlling the stoichiometry allows one to do this.

Table 1. List of MBE - grown and sputtered Bi-Te and Sb-Te thin films. The Te contents shown here were determined by SEM-EDX. Full details of synthesis are given in cited references. The samples with ID numbers as indicated in the fourth column are identical to the corresponding samples in the cited references.

Sample No.	Nominal composition	Te [at%]	ID	Ref.
Nominally stoichiometric MBE grown films on SiO_2 substrates				
1	Sb_2Te_3	61.0	ST-S2	[11]
2	Bi_2Te_3	59.1	BT-S2	[11]
Stoichiometry series of MBE grown Bi-Te films on BaF_2 substrates				
3	Bi_2Te_3	59.4	BT-B2, BT-Q	[11,14]
4	Bi-Te with Bi excess	52.3	BT-Q	[14]
5	Bi-Te with Te excess	61.8	BT-Q	[14]
Nominally stoichiometric sputtered films on BaF_2 substrates				
6	Sb_2Te_3	60.2		[12]
7	Bi_2Te_3	62.1		[13]

The thermopower of MBE-grown films follows the charge-carrier densities nicely in sign and value, with maximum values of –182 μV K^{-1} for n-type films and 130 μV K^{-1} for p-type films. The mobilities measured in these samples differ significantly, the mobilities are low for the Bi_2Te_3 thin films and are much higher for Sb_2Te_3. As a trend the mobilities decrease with increasing charge-carrier density.

The sputtered films of Bi_2Te_3 were n-type whereas those of Sb_2Te_3 were p-type, and the charge-carrier densities were slightly higher than in MBE-grown films. Note that particularly for Sb_2Te_3 both deposition methods yield lower charge-carrier densities as compared to those of bulk samples.

Table 2. In-plane transport measurements of MBE - grown and sputtered Bi-Te and Sb-Te thin films measured at room temperature: charge-carrier density n, thermopower S, charge-carrier mobility μ, electrical conductivity σ, and power factor $S^2\,\sigma$. Carrier density values with a negative sign indicate electron conduction, a positive sign indicates hole conduction.

Sample No.	Nominal composition	n [cm^{-3}]	S [μV K^{-1}]	μ [cm^2 V^{-1} s^{-1}]	σ [Ω^{-1} cm^{-1}]	$S^2\,\sigma$ [μW cm^{-1} K^{-2}]
Nominally stoichiometric MBE grown films on SiO_2 substrates						
1	Sb_2Te_3	2.60×10^{19}	130	402	1696	29
2	Bi_2Te_3	-2.74×10^{19}	–153	80	338	8
Stoichiometry series of MBE grown Bi-Te films on BaF_2 substrates						
3	Bi_2Te_3	-2.74×10^{19}	–182	61	270	9
4	Bi-Te with Bi excess	-4.27×10^{20}	–56	25	1688	5
5	Bi-Te with Te excess	-1.16×10^{20}	–112	29	547	7
Nominally stoichiometric sputtered films on BaF_2 substrates						
6	Sb_2Te_3	7.88×10^{19}	110	182	2290	28
7	Bi_2Te_3	-5.69×10^{19}	–163	80	731	19

2.2. Chemical Analysis by WDX Spectrometry

WDX spectrometry was used to determine the chemical composition of the films. Antisite defects yield changes in the mole fraction and can in principle be traced by this method. For high-accuracy analysis it is essential to perform data acquisition and analysis with great care, details of this are given in the Experimental Section and the Supporting Information. Most analyses so far have been carried out by EDX spectrometry, however, the benefits of WDX analysis with respect to EDX are well known and the reader is referred to text books on that issue.[18] WDX spectrometry has been carried out on Bi_2Te_3-based bulk samples,[19] which has demonstrated the high potential of this measurement technique.

The results of the chemical analysis of the films are summarized in **Figures 1–3** and **Table 3**. Note that apart from detecting the main elements contamination of the films by oxygen (MBE) and Ar (in sputtered films) could also clearly be seen. The mole fractions of the contaminants were 4–9 at% for oxygen (Figure 2) and up to 0.8 at% for Ar (Figure 3a). Particularly for Ar only WDX spectrometry yields adequate minimum detectable mass fractions and a large peak-to-background ratio (Figures 2c,d), whereas EDX spectrometry does not (Figures 2a,b) because of its poor energy resolution.

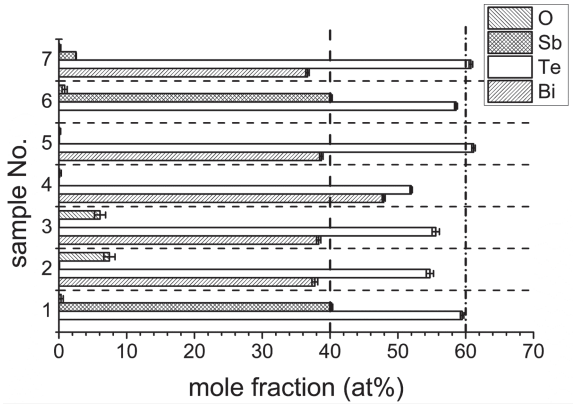

Figure 1. Chemical compositions of Bi-Te and Sb-Te thin films determined by WDX spectrometry. The dashed vertical lines indicate the stoichiometric mole fractions for Bi_2Te_3 and Sb_2Te_3. The error bars indicate variations in stoichiometry.

MBE-grown and sputtered Sb_2Te_3 films were found to be stoichiometric (samples 1 and 6). Oxygen contamination was found in MBE-grown Bi_2Te_3 films that were nominally close to stoichiometry (samples 2 and 3). The sputtered Bi_2Te_3 film (sample 7) that was stoichiometric with respect to Te was slightly contaminated by Sb. EDX analysis of the MBE-grown films as published in the references quoted in Table 1 indicated stoichiometric films and did not provide this important information. Only by EDX spectrometry carried out in a transmission electron microscope (TEM) it was realized that oxidized grain boundary layers do exist.[11] Also sputtered films were analyzed by EDX but neither Sb nor Ar contamination could be detected. Therefore, this paper provides detailed chemical analysis as well as highlights the advantage of WDX analysis over EDX.

3. Discussion

3.1. Transport Properties

A detailed discussion of the transport properties of nominally stoichiometric MBE-grown films has been given in a previous report. [11]

In this paper we concentrate on results that also cover non-stoichiometric films and investigate the effect of the contamination particularly in nominally stoichiometric films deposited both by MBE and sputtering. The obtained results will also be compared to data obtained from bulk samples and to calculations based on Boltzmann transport theory.

Transport theory predicts for Bi_2Te_3 a very sensitive dependence of the thermopower on the charge-carrier density as shown in **Figure 4**. Results of Bi-Te bulk compounds[1,15] show that Bi-rich samples are p-type and Te-rich samples are n-type conducting, which is nicely matched by the calculations (Figure 4). Note that p-type Bi_2Te_3 thin films could not be obtained (Figure 4) by the thin-film preparation technology although the Te content was varied from 52.3 at% to 61.8 at%.[14]

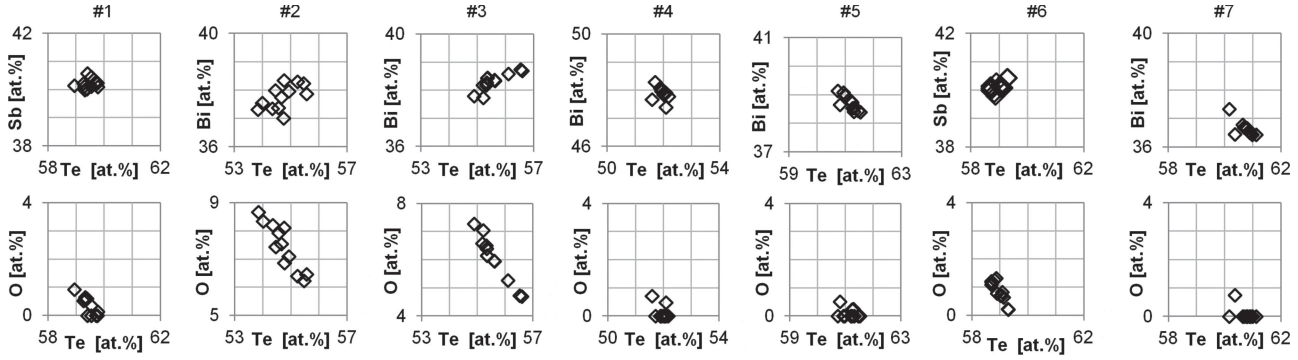

Figure 2. Correlation diagrams obtained after quantitative analysis of WDX spectra obtained from Bi-Te and Sb-Te thin films. A strong oxidation and a negative Te-O correlation is observed in Bi_2Te_3 thin films #2 and #3.

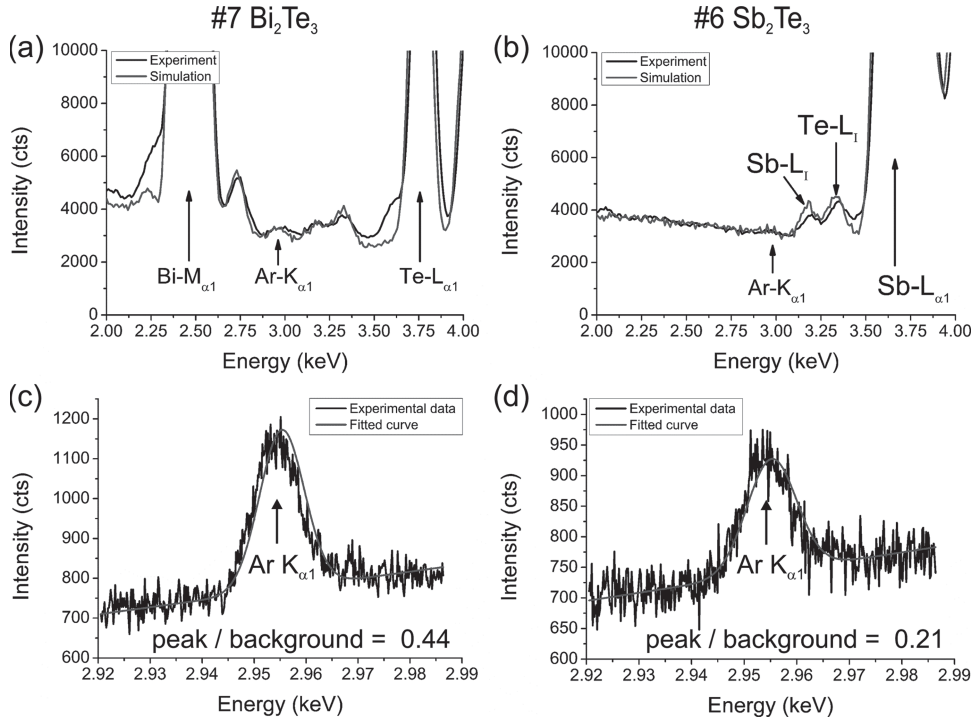

Figure 3. a,b) Evaluation of Ar content in sputtered Bi_2Te_3 and Sb_2Te_3 thin films by comparing experimental SEM-EDX spectra (black lines) and Monte Carlo simulations (red lines), yielding 0.8 at% Ar in Bi_2Te_3 film and 0.4 at% Ar in Sb_2Te_3 film. c,d) WDX spectra acquired at the Ar K_1 X-ray line in the same thin films.

We believe that the annealing conditions play a major role for this to happen, this will be discussed in more detail in the next section. In summary, thin films with charge-carrier densities as low as 3×10^{19} cm^{-3} could be synthesized by the applied technology. This low charge-carrier density is necessary to reach the maximum values of the thermopower.

Oxidation of the films could be proven both by WDX measurements (this paper) and by analytical TEM, yielding oxidized Bi-rich secondary phases at grain boundaries.[11] Despite significant oxidation the thermopower and charge-carrier density values of samples 2 and 3 match satisfactorily those of BoltzTraP simulations (Figure 4).[21,22] Therefore, oxygen-rich secondary phases have a minor effect on the relation between the macroscopic thermopower and the charge-carrier density. However, these secondary phases are assumed to severely reduce charge-carrier mobility.[11] Note the large deviations of relations between electrical conductivity and charge-carrier density values for Bi-Te thin films in contrast to BoltzTraP simulations and experimental bulk values.

Table 3. Mean chemical compositions and sum of mass fractions of MBE grown and sputtered Bi-Te and Sb-Te thin films as determined by WDX spectrometry.

Sample No.	Nominal composition	Bi [at%]	Sb [at%]	Te [at%]	O [at%]	Sum wt%
	Nominally stoichiometric MBE grown films on SiO_2 substrates					
1	Sb_2Te_3		40.21	59.47	0.31	98.69
2	Bi_2Te_3	37.76	0.05	54.72	7.45	98.24
	Stoichiometry series of MBE grown Bi-Te films on BaF_2 substrates					
3	Bi_2Te_3	38.32	0.02	55.58	6.07	98.52
4	Bi-Te with Bi excess	47.91	0.01	51.96	0.10	98.00
5	Bi-Te with Te excess	38.71	0.03	61.15	0.08	98.14
	Nominally stoichiometric sputtered films on BaF_2 substrates					
6	Sb_2Te_3		40.13	58.56	0.85	98.42
7	Bi_2Te_3	36.64	2.52	60.76	0.06	99.42

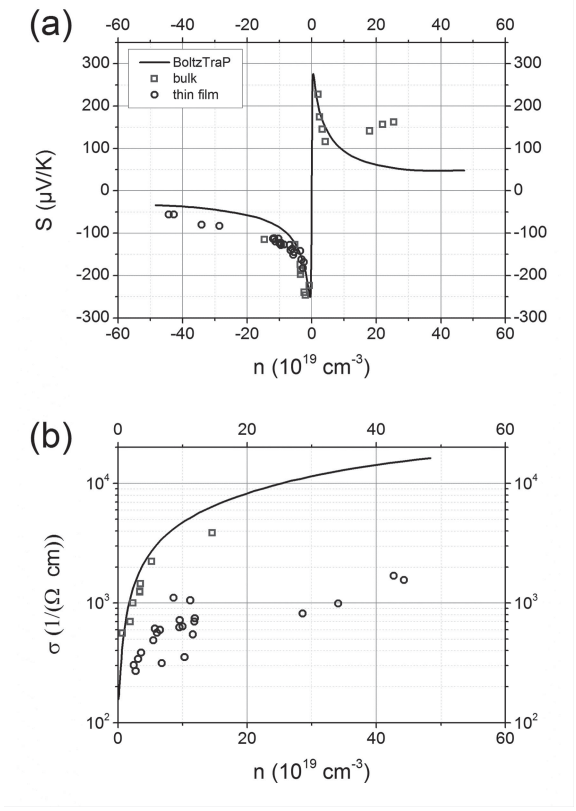

Figure 4. Dependence of a) thermopower S andb) electrical conductivity σ on charge-carrier density n for Bi-Te materials. Blue circles indicate in-plane values obtained from a stoichiometric series of MBE-grown thin films with a Te content between 52.3 at% and 61.8 at%,[14] values of samples #3, #4, and #5 are also included. Red squares indicate basal plane values of bulk samples with a Te content between 51.5 at% and 70.5 at%.[1,15] Solid lines indicate basal plane transport properties of Bi_2Te_3 as a function of the chemical potential calculated by solving the linearized Boltzmann equation.[21,22]

For studying the oxidation in more detail we generated Te vs. O correlation diagrams. These clearly show that Te and oxygen are negatively correlated in MBE-grown Bi_2Te_3 films (Figure 2, samples 2 and 3) and, therefore, oxygen substitutes Te.

3.2. Antisite Defects and Their Effects on Transport Properties

Bi_{Te} and Te_{Bi} antisite defects are the most dominant point defects in Bi-Te materials because of their low formation energies,[23,24] with Bi occupying Te sites (Bi_{Te}) in Bi-rich materials and Te occupying Bi sites (Te_{Bi}) in Te-rich materials. Bi-rich bulk materials reveal p-type conduction (Figure 4) as Bi_{Te} antisites act as acceptors. However, Bi-rich thin films grown by MBE yielded n-type conduction (Figure 4). Therefore, the point defect model for Bi-rich bulk does not hold for these thin films. The synthesis temperature has to be considered for calculating point-defect densities.[10] Miller and Li[16] used for stoichiometric bulk the expression

$$\mu = -k_B T_m(\ln([A]/[Te]) + 1), \quad (1)$$

Table 4. Measured and calculated charge-carrier densities for Bi-Te thin films with Te excess assuming that non-stoichiometry is compensated only by Te_{Bi} antisite defects and the number of Te_{Bi} antisite defects is equal to the number of electrons.

Sample No.	Te [at%]	$n_{measured}$ [cm^{-3}]	$n_{calculated}$ [cm^{-3}]
5	61.15 ± 0.25	-1.16×10^{20}	$-3.40 \times 10^{20} \pm 0.73 \times 10^{20}$
7	60.76 ± 0.21	-5.69×10^{19}	$-2.24 \times 10^{20} \pm 0.62 \times 10^{20}$

where μ is the formation energy, T_m the melting point, [A] the antisite density, and [Te] the Te site density. Bi_2Te_3 bulk is grown from a melt at 585 °C;[1] however, thin films are exposed to a maximum annealing temperature of 250 °C. According to Equation 1 this yields low densities of antisite defects ($<10^{17}$ cm^{-3}) and charge carriers.[10]

Te-rich bulk materials reveal n-type character (Figure 4) as Te_{Bi} antisites act as donors.[16,23,25] For Te-rich films grown by MBE the Te_{Bi} antisite defect density was calculated assuming that the non-stoichiometry is compensated only by antisite defects. From the chemical composition as determined by high-accuracy WDX the antisite defect concentration can be calculated according to

$$[Te_{Bi}] = [Te]/60\ \text{at\%}(C_{Te} - 60\ \text{at\%}), \quad (2)$$

where C_{Te} is the measured Te mole fraction in at% and [Te] is the volume density of Te sites. We assumed that each Te_{Bi} antisite defect yields one additional electron in the conduction band in the case of Te excess.[16] The calculated values for the charge-carrier density are 3–4 times larger than the measured values (**Table 4**), indicating that only a fraction of the Te_{Bi} antisite defects are electrically active. Note that this is the first time that precise chemical analysis is used for determining antisite defect concentrations experimentally. In the paper of Miller and Li the weight of the bulk sample was used for determining the antisite defect concentration. This method cannot be applied for thin films.

3.3. Impurities and Their Effects on Transport Properties

Oxygen substitutes Te in MBE-grown Bi_2Te_3 films (Figure 2, samples 2 and 3). On the other hand, TEM revealed oxidized Bi-rich blocking layers at the grain boundaries,[11] which are assumed to severely reduce the charge-carrier mobility.[11,26] Therefore, oxygen seems to substitute Te in the blocking layers and presumably to a lesser extent also in the matrix.

Oxygen is known to turn bulk Bi_2Te_3 from a p-type to an n-type material;[27] however, no detailed explanation has thus far been given as to why this should be the case.

The thermoelectric properties of n-type $Bi_2Te_{2.7}Se_{0.3}$ materials prepared by the hot pressing technique have been measured systematically depending on the amount of oxygen contamination.[28,29] The as-solidified material yielded 0.04 at% oxygen and a thermopower of –232 μV K^{-1}. The as-sintered material yielded 1.8 at% oxygen and a significantly reduced thermopower of –135 μV K^{-1}. Subsequent reduction of the

sintered material by hydrogen yielded 0.25 at% oxygen and a thermopower of –215 μV K^{-1} was recovered.

Also by alloying with other group 6 elements the electrical properties of Bi_2Te_3 have been affected. $Bi_2(Te_{1-x}Se_x)_3$ and $Bi_2(Te_{1-x}S_x)_3$ mixed crystals are known to switch from p-type to n-type character for 13 at% Se and 2.4 at% S, respectively.[25,30] According to Horák et al.[25] the hole concentration decreases with increasing mole fraction of Se and S in the anion sublattice, which presumably increases the anion vacancy concentration (V_A^{-2} donors). This increase was explained by a reduced vacancy formation energy due to the smaller effective radius of the anions. Therefore, $Bi_2(Te_{1-x}S_x)_3$ yielded higher anion vacancy concentrations and a transition from p- to n-type character occurs at smaller x than for $Bi_2(Te_{1-x}Se_x)_3$ mixed crystals. Similar arguments hold for $Bi_2(Te_{1-x}O_x)_3$, explaining why the transport properties change so drastically for small oxygen contents.

Bulk materials with Bi excess yield p-type conduction (Figure 4),[1,15] which is explained by acceptor-like Bi_{Te} antisites.[16] However, in the series of Bi-Te thin films with Bi excess investigated here only n-type conduction was observed, which is in agreement with similar reports.[5,9,10,31] The chemical analysis of such films revealed about 7 at% oxygen in some Bi-Te films (samples 2 and 3), which might explain their n-type character. However, n-type films were found to have a large Bi concentration of 48 at% Bi but only 0.1 at% O (sample 4). This supports a previous hypothesis[10] that the low substrate and annealing temperatures (250 °C) that are applied to the thin films investigated here yield significantly different point-defect concentrations than the congruent melting point (585 °C) used to prepare bulk structures.

In summary, these results show that the thermoelectric properties are sensitive to oxidation and thus the samples require careful protection from contamination during synthesis and an accurate chemical analysis for understanding their thermoelectric properties. The sputtered Bi_2Te_3 film (sample 7) yielded a significantly reduced oxygen contamination (Table 3) as compared to the MBE-grown Bi_2Te_3 film (sample 2) as a small leak in the annealing setup could be closed. However, both films yielded the same low charge-carrier mobility (Table 2). An analytical TEM study[11] of the nanostructure in the sputtered Bi_2Te_3 film is required to explain its low mobility although the oxygen contamination problem was solved.

This paper also reports on Ar incorporation into sputtered Bi_2Te_3 thin films that can only be detected by WDX spectrometry. The solubility of Ar is large and has been found to be larger in Bi_2Te_3 (0.8 at%) than in Sb_2Te_3 (0.4 at%), which is likely related to the larger lattice parameters of Bi_2Te_3.[1] Argon might occupy sites in the van der Waals layer of the structure. Argon point defects will introduce strain and thereby reduce the lattice thermal conductivity. Argon incorporation is an intrinsic effect of sputtering and, therefore, will affect the transport properties.

The effect of Ar irradiation in Bi_2Te_3 has been studied systematically.[32] It was found that Ar irradiation in the keV range gives rise to the formation of a structural modulation with a wavelength of 10 nm and yields exciting new possibilities for phonon scattering in this material. Also, in alumina thin films deposited by sputtering Ar allows to stabilize the cubic γ–phase rather than the α–phase.[33]

Horák and collaborators[24,25] showed that substituting Bi with Sb only slightly changes the charge-carrier density. Therefore, a Sb contamination with mole fractions of about 2 at% as observed here will hardly affect the transport properties.

3.4. High-Accuracy Chemical Analysis for Growth of Stoichiometry Controlled Thin Films

In this paper we have shown that high-accuracy chemical analysis by WDX is of paramount importance for stoichiometry control, calibration of growth parameters, and finally production of high-ZT materials.

Choosing the right acquisition parameters is essential as the electron energy determines the excitation volume. The acceleration voltage should be chosen such that electrons only penetrate the film but not the substrate. This can only be guaranteed by detailed Monte Carlo simulations[34] of the electron trajectories as explained in more detail in the Supporting Information of the paper. The analysis of Sb_2Te_3 is much more difficult than that of Bi_2Te_3 as Sb and Te are neighbors in the periodic table and significant peak overlap occurs. If all these points are taken into consideration adequately then high-accuracy measurements result, yielding a sum of mass fractions close to 100 wt% (Table 3).

In summary, the better energy resolution of WDX (10 eV) as compared to EDX (135 eV) spectrometry yielded a smaller peak -overlap and high peak-to-background ratios and thus low detection limits, which are of key importance for analyzing contamination of for instance Ar in sputtered films.

Small deviations (<0.5 at%) between EDX and WDX occurred for not oxidized Bi-Te films (samples 4, 5, and 7), which can be seen by comparing theTe mole fractions in Table 1 and 3, respectively. Larger deviations (1<at%) were found for Sb_2Te_3 films (samples 1 and 6) because of the peak overlap of the Sb and Te peaks. The largest deviations (>2 at%) were found in oxidized Bi_2Te_3 films (samples 2 and 3) and because of Sb contamination in sputtered Bi_2Te_3 films, which was only detected by WDX spectrometry.

4. Conclusions

The charge-carrier densities are governed by antisite defects in Bi_2Te_3 thermoelectric materials. In this work the effect of point defects on electrical transport was investigated by a combined approach of chemical analysis and calculating transport coefficients. WDX spectrometry was applied to measure precisely the chemical composition. In Te-rich thin films the Te_{Bi} antisite defect concentration was determined, assuming that non-stoichiometry is only compensated by this type of point defect. Finally, the charge-carrier density was calculated assuming that the number of electrons is equal to the number of Te_{Bi} antisite defects. Thermopower and electrical conductivity were calculated as a function of charge-carrier density by solving the linearized Boltzmann transport equation. WDX spectrometry has improved spectral resolution with respect to EDX, which is usually applied, and, therefore, has a high impact for improving thin-film quality. Even large dopant concentrations

in semiconductors can be measured by WDX with even better accuracy than antisite defects. Therefore, this approach is useful for many other applications based on thin films.

Bi_2Te_3 and Sb_2Te_3 thin films grown by sputtering and MBE yielded low charge-carrier densities, for such films chemical analysis yielded a near stoichiometric composition. Good quantitative agreement was found for the dependence of the thermopower on stoichiometry. The Ar content in sputtered films was measured for the first time and was found to be about 1 at%.

In summary, WDX spectrometry is a powerful technique for chemical analyses of thin films used for various applications. In particular, the control of stoichiometry, point-defect densities, impurity concentrations, and transport properties by WDX is of key importance for Bi_2Te_3-based nanomaterials used for thermoelectric applications and topological insulators.

5. Experimental Section

Three different types of binary Bi_2Te_3 and Sb_2Te_3 thin films with thicknesses of 1 µm were grown (Table 1): i) Nominally stoichiometric Bi_2Te_3 and Sb_2Te_3 thin films were deposited on SiO_2 substrates using a MBE setup (samples 1 and 2, respectively). ii) A stoichiometric series of Bi-Te thin films were deposited on BaF_2 substrates using a MBE setup with Te contents between 52.3 at% Te and 61.8 at% as determined by EDX in a scanning electron microscope. In this paper only a near-stoichiometric sample and samples with lowest and highest Te contents were selected from this series for chemical analysis (samples 3, 4, and 5, respectively). iii) Nominally stoichiometric Bi_2Te_3 and Sb_2Te_3 thin films were sputtered on BaF_2 substrates (samples 6 and 7, respectively). For MBE deposition and sputtering a growth procedure referred to as nano-alloying was applied, this means that films were deposited at room temperature and subsequently annealed at 250 °C for 2 h for phase formation; details of the deposition methods are described in the references quoted in Table 1.

In thin films the in-plane transport properties (charge-carrier density n, charge-carrier mobility µ, electrical conductivity σ, and thermopower S) were measured at room temperature; experimental details are reported elsewhere (see references in Table 1).

X-ray diffraction (XRD), scanning electron microscopy (SEM), energy-filtered transmission electron microscopy (TEM), and energy-dispersive X-ray spectrometry (EDX) were applied to the nominally stoichiometric films (#1, #2, #3, #6, #7) to monitor the crystal structure, texture, chemical composition, grain size, and extended crystal defects. Details about the instruments, specimen preparation, and acquisition conditions were explained in previous reports (see references in Table 1).

Chemical analysis of the films was conducted with wavelength-dispersive X-ray spectrometry (WDX) in an electron-probe microanalyzer (EPMA) and energy-dispersive X-ray spectrometry (EDX) in a scanning electron microscope (SEM). The size of the excitation volume was determined by Monte Carlo simulations of electron trajectories in 1-µm thick Bi_2Te_3 and Sb_2Te_3 films using the Desktop Spectrum Analyzer (DTSA-II) software.[34] Details are explained in the Supporting Information. It was found that for electron energies less than 15 keV the electrons will not reach the substrate and, therefore, the X-ray spectra will particularly not contain O-K stray radiation generated in the SiO_2 substrates.

For WDX analysis a JEOL JXA Superprobe 8900 was used operated at 10 keV, a probe current of 17.2 nA, and a beam size of 5 µm. For each film 10 measurements were carried out. PbTe, Bi, Al_2O_3, and InSb compounds were used as standards and the φ–ρ-z method[18] was applied for quantitative analysis. The acquisition times were between 30 s and 60 s in order to obtain minimum statistical errors with following netcounts/ detection limits for the various X-ray lines: 20 000/ 600 ppm for Bi-$M_{\alpha 1}$, 200 000/ 300 ppm for Te-$L_{\alpha 1}$, 150 000/ 250 ppm for Sb-$L_{\alpha 1}$ and <1000/ 900 ppm for O-$K_{\alpha 1}$. A peak-overlap correction was applied for the Te and Sb lines and turned out be essential for finally yielding a sum of all mass fractions between 98% and 99.4% (Table 1). This indicates the high quality of the performed measurements.

WDX was also used for detection of Ar in sputtered films, for these measurements the acquisition time was set to 1 h. The Ar content was quantitatively analyzed by combined SEM-EDX analysis and Monte Carlo simulations.[34] The EDX spectra were acquired in a JEOL JSM 6500F scanning electron microscope operated at 12 kV and with a probe current of 80 pA. The spectra were acquired in area scanning mode (5 µm × 5 µm) to avoid contamination and with an acquisition time of 2000 s.

Electronic transport coefficients of Bi_2Te_3 for transport along the basal plane were calculated by solving the linearized Boltzmann transport equation using the BoltzTraP code.[21] The band structure used was provided by the BoltzTraP code and was that published by Scheidemantel et al.,[22] calculated by the WIEN2K software.[35] Texture analysis of the films revealed that in-plane transport properties can approximately be understood as basal plane properties and, therefore, these quantities will be compared.[11–14]

Supporting Information

Supporting Information is available from the Wiley Online Library or from the author.

Acknowledgements

Financial support by the German Research Foundation (DFG), Priority Program 1386 "Nanostructured Thermoelectric Materials: Theory, Model Systems and Controlled Synthesis" is gratefully acknowledged. We thank Dr. Thomas Wenzel from the Institute of Mineralogy, Petrology, and Geochemistry for help with the WDX measurements.

Received: February 16, 2013
Published online: April 26, 2013

[1] D. M. Rowe, *CRC Handbook of Thermoelectrics*, CRC, Boca Raton, FL **1995**, Ch. 19.
[2] L. D. Hicks, M. S. Dresselhaus, *Phys. Rev. B* **1993**, *47*, 16 631–16 634.
[3] J. E. Cornett, O. Rabin, *Appl. Phys. Lett.* **2011**, *98*, 182 104.
[4] R. Venkatasubramanian, E. Siivola, T. Colpitts, B. O'Quinn, *Nature* **2001**, *413*, 597–602.
[5] B. Huang, C. Lawrence, A. Gross, G.-S. Hwang, N. Ghafouri, S.-W. Lee, H. Kim, C.-P. Li, C. Uher, K. Najafi, M. Kaviany, *J. Appl. Phys.* **2008**, *104*, 113 710.
[6] L. W. da Silva, M. Kaviany, C. Uher, *J. Appl. Phys.* **2005**, *97*, 114 903.
[7] L. M. Goncalves, C. Couto, P. Alpuim, A. G. Rolo, F. Völklein, J. H. Correia, *Thin Solid Films* **2010**, *518*, 2816–2821.
[8] H. Zou, D. M. Rowe, S. G. K. Williams, *Thin Solid Films* **2002**, *408*, 270–274.
[9] N. Peranio, O. Eibl, J. Nurnus, *J. Appl. Phys.* **2006**, *100*, 114 306.
[10] N. Peranio, M. Winkler, Z. Aabdin, J. König, H. Böttner, O. Eibl, *Phys. Status Solidi A* **2012**, *209*, 289–293.
[11] N. Peranio, M. Winkler, D. Bessas, Z. Aabdin, J. König, H. Böttner, R. P. Hermann, O. Eibl, *J. Alloy. Compd.* **2012**, *521*, 163–173.
[12] M. Winkler, X. Liu, J. D. König, L. Kirste, H. Böttner, W. Bensch, L. Kienle, *J. Electron. Mater.* **2012**, *41*, 1322–1331.
[13] M. Winkler, J. D. König, S. Buller, U. Schürmann, L. Kienle, W. Bensch, H. Böttner, *Proc. 8th Eur. Conf. Thermoelectrics*, Como, Italy, **2010**, article I-V.

[14] M. Winkler, X. Liu, J. D. König, S. Buller, U. Schürmann, L. Kienle, W. Bensch, H. Böttner, *J. Mater. Chem.* **2012**, *22*, 11 323–11 334.
[15] J. P. Fleurial, L. Gailliard, R. Triboulet, H. Scherrer, S. Scherrer, *J. Phys. Chem. Solids* **1988**, *49*, 1237–1247.
[16] G. R. Miller, C.-Y Li, *J. Phys. Chem. Solids* **1965**, *26*, 173–177.
[17] C. Drasar, P. Lostak, C. Uher, *J. Electron. Mater.* **2010**, *39*, 2162–2164.
[18] V. D. Scott, G. Love, S. J. B. Reed, *Quantitative Electron Probe Microanalysis*, 2nd ed., Ellis Horwood, New York, NY **1995**.
[19] D. Eyidi, D. Maier, O. Eibl, M. Westphal, *Phys. Status Solidi A* **2001**, *1187*, 585–600.
[20] N. Peranio, O. Eibl, *Phys. Status Solidi A* **2007**, *204*, 3243–3255.
[21] G. K. H. Madsen, D. J. Singh, *Comput. Phys. Commun.* **2006**, *175*, 67–71.
[22] T. J. Scheidemantel, C. Ambrosch-Draxl, T. Thonhauser, J. V. Badding, J. O. Sofo, *Phys. Rev. B* **2003**, *68*, 125 210.
[23] A. Hashibon, C. Elsässer, *Phys. Rev. B* **2011**, *84*, 144 117.
[24] J. Horák, K. Čermák, L. Koudelka, *J. Phys. Chem. Solids* **1986**, *47*, 805–809.
[25] J. Horák, Z. Starký, J. Votinský, *Philos. Mag. B* **1994**, *69*, 31–38.
[26] Y. Horio, A. Inoue, *Mater. Trans.* **2006**, *47*, 1412–1416.
[27] J. M. Schultz, J. P. McHugh, W. A. Tiller, *J. Appl. Phys.* **1962**, *33*, 2443–2450.
[28] C. H. Lim, D. C. Cho, Y. S. Lee, C. H. Lee, K. T. Kim, D. M. Lee, *J. Korean Phys. Soc.* **2005**, *46*, 995–1000.
[29] D. C. Cho, C. H. Lim, D. M. Lee, S. Y. Shin, C. H. Lee, *Mater. Sci. Forum* **2004**, 449–452, 905–908.
[30] U. Birkholz, *Z. Naturforsch.* **1958**, *13a*, 780–792.
[31] A. Taylor, C. Mortensen, R. Rostek, N. Nguyen, D. C. Johnson, *J. Electron. Mater.* **2010**, *39*, 1981–1986.
[32] N. Peranio, Z. Aabdin, O. Eibl, *Adv. Mater.* **2012**, *24*, 4605–4608.
[33] W. Engelhart, W. Dreher, O. Eibl, V. Schier, *Acta Mater.* **2011**, *59*, 7757–7767.
[34] N. Ritchie, *Microsc. Microanal.* **2009**, *15*, 454–68.
[35] P. Blaha, K. Schwarz, G. K. H. Madsen, D. Kvasnicka, J. Luitz, *WIEN2k, An Augmented Plane Wave + Local Orbitals Program for Calculating Crystal Properties*, Karlheinz Schwarz, Technische Universität Wien, Austria **2001.**